RSC Advances

ROYAL SOCIETY OF CHEMISTRY

www.rsc.org/advances

Journal Name

COMMUNICATION

Orientation-Controlled $BaTiO_3$ Thin Films Fabricated by Chemical Solution Deposition

Tadasu Hosokura,[a] * Akira Ando,[a] and Takehiro Konoike[a]

Received 00th January 20xx,
Accepted 00th January 20xx

DOI: 10.1039/x0xx00000x

www.rsc.org/

We synthesized orientation-controlled (100), (110), and (111) $BaTiO_3$ films by the chemical solution deposition method. The electric properties of the fabricated $BaTiO_3$ thin films were evaluated, and dielectric constants of 2000 were found for the (110)-oriented and (111)-oriented $BaTiO_3$ film, with temperature dependence stabilized from 20 °C to 150 °C.

Barium titanate ($BaTiO_3$) thin films are of significant interest as ferroelectric materials for the fabrication of ferroelectric memory devices,[1,2] multilayer capacitors,[3] optical modulators,[4] and other devices. Recently, high-quality ferroelectric thin films have been used in advanced microwave signal-processing devices, and small, compact, and low-power microwave devices, including phase shifters, tunable filters, tunable resonators, phased array antennas, and frequency agile microwave radio transceivers, have been fabricated from structures based on ferroelectric films. $BaTiO_3$ thin films satisfy most device requirements because of their unique properties.

$BaTiO_3$ thin films have been prepared by various techniques, such as RF sputtering,[5,6] pulsed laser deposition,[7-10] metal-organic chemical vapor deposition (MOCVD),[11-14] and chemical solution deposition (CSD) processing.[15] Among these methods, CSD processing is preferred because it requires simple and inexpensive equipment and offers good homogeneity, chemical composition control, high purity, low processing temperature, and large applicable areas.[16]

In recent years, there has been increasing interest in enhancing ferroelectric behavior by inducing strain, such as through the synthesis of artificial superlattices of oxide materials, control of substrate thermal expansion coefficients, and control of the layer orientation.[17-22] We synthesized epitaxially grown $SrTiO_3(100)/BaTiO_3(100)$ artificial superlattices on Pt(100)/MgO(100) substrates by a chemical solution deposition method to improve the substrate's dielectric properties by inducing a mismatch between the $SrTiO_3$ and $BaTiO_3$ layers.[23] However, the lattice mismatch also induced defects between the $SrTiO_3$ and $BaTiO_3$ layers that relaxed the misfit strain, and the ferroelectric behavior enhancement was weakened as the strain was relaxed.

According to the first principle calculation of a (110)-oriented $BaTiO_3$ film as a function of the misfit strain, the compressive biaxial strain enhanced the dielectric constant relative to the dielectric constant of the (100)-oriented $BaTiO_3$.[24] Unusual features were discovered that significantly differed from those found in $BaTiO_3$ films grown along the "usual" [001] direction. The (110)-oriented $BiFeO_3$ film also exhibited a large polarization caused by the uniaxial strain.[17]

Although CSD of $BaTiO_3$ typically results in a poly-crystalline, granular film because of the trend toward homogeneous nucleation in the pyrolyzed precursor,[25-27] the CSD process is applicable for fabricating epitaxially grown $BaTiO_3$ films. One-axis-oriented columnar micro-structured $BaTiO_3$ (111) films and (100)-oriented $BaSrTiO_3$ films have also been fabricated by the CSD process.[28-30]

However, the orientation of these films was not highly controlled, so the results of these studies were not applicable for evaluating the enhancement of ferroelectric behavior by controlling orientation of the $BaTiO_3$ film. Here, we present the fabrication of (100)-, (110)-, and (111)-oriented $BaTiO_3$ films on Pt coated MgO substrates by CSD processing. The electric properties of the fabricated $BaTiO_3$ thin films were evaluated, and differences in the electric properties caused by the orientation of the $BaTiO_3$ were considered.

A Pt(100)/MgO(100) substrate, Pt(110)/MgO(110) substrate, and Pt(111)/MgO(111) substrate were used to fabricate the $BaTiO_3$ thin films by the CSD method. The Pt(100), Pt(110), and Pt(111) films were epitaxially grown on a 15 x 15 mm size

[a] *Murata Manufacturing Co., Ltd.*
10-1, Higashikotari, 1-chome, Nagaokakyo-shi, Kyoto 617-8555 Japan.
E-mail:hosokura@murata.com

† Electronic Supplementary Information (ESI) available: [Figure S1 cross-sectional FE-SEM image of the BaTiO3 films; Figure S2-S4 cross-sectional TEM images of the $BaTiO_3$ films; Table S1 Elastic constants and tensile stress in the plane of the growth direction of (100)-, (110)-, and (111)-oriented film. ; Table S2 the capacitance of the obtained $BaTiO_3$ films measured at 1 kHz and 0.1 V. ; Table S3 DC resistivity of thin films prepared from a variety of film orientations measured at 300 kV/cm.] See DOI: 10.1039/x0xx00000x

MgO(100), MgO(110), and MgO(111) wafer, respectively, at 600 °C by DC sputtering. A 0.07 M chemical solution was prepared by dissolving $Ba(CH_3COO)_2$ and $Ti(O\text{-}i\text{-}C_3H_7)_4$ at a 1:1 molar ratio in a mixed solvent of acetic acid and ethylene glycol monoethyl ether. The chemical solution was deposited by dispersing it on the substrate, and then spin coating was performed at 4000 rpm for 50 s. Subsequently, the films were dried on a hot plate at 150 °C for 3 min. The dried and coated films were annealed by RTA at 800 °C for 30 min at a heating rate of 300 °C/min under an oxygen atmosphere. To prepare the $BaTiO_3$ thin films, the deposition procedure was repeated 20 times. Pt dots were sputtered by placing a 25 holes opened stainless mask with a diameter of 0.5 mm on the $BaTiO_3$ thin films to form metal_dielectric_metal (MDM) capacitors, which were used to investigate their dielectric nature.

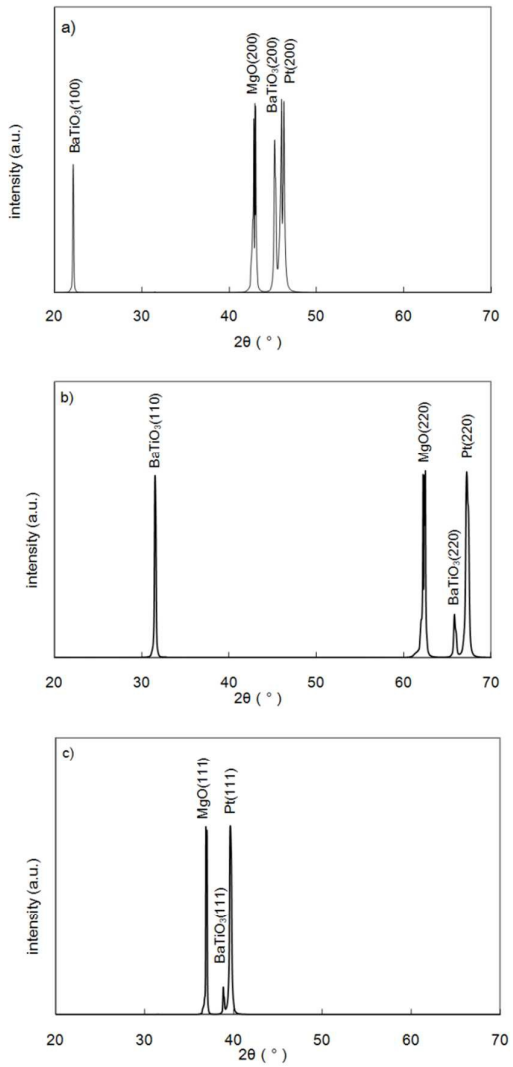

Fig. 1 The XRD pattern of (a) $BaTiO_3$(100) film on a Pt(100)/MgO(100) substrate, (b) $BaTiO_3$(110) film on a Pt(110)/MgO(110) substrate, and (c) $BaTiO_3$(111) on a Pt(111)/MgO(111) substrate.

Figure 1 (a) shows the XRD pattern of the $BaTiO_3$(100). In figure 1(a), the four peaks at 22.3°, 42.9°, 45.4°, and 46.4° are attributable to $BaTiO_3$(100) (cubic; JCPDS: 31-0174), MgO(200) (JCPDS: 45-0946), $BaTiO_3$(200), and Pt (JCPD: 04-0802) (200) refractions, respectively. The lattice constants of the $BaTiO_3$ films were calculated from the obtained XRD results by assuming that the crystal structure of the $BaTiO_3$ is cubic perovskite. The attributed peaks indicate that the perovskite $BaTiO_3$(100) was heteroepitaxially grown on the Pt(100)/MgO(100). The lattice constant of the $BaTiO_3$(100) film was calculated to be 0.4060 nm. Lattice constant of cubic perovskite $BaTiO_3$ is well known to be 0.400 nm which is likely equal to the lattice constant of the $BaTiO_3$(100) film.[31] Compared with the tetragonal perovskite $BaTiO_3$ peaks (JCPD: 07-9164), the $BaTiO_3$ thin films were confirmed to pseudocubic perovskite $BaTiO_3$ because the 200 peak does not showing any splitting. Figure 1 (b) shows the XRD pattern of the $BaTiO_3$ deposited on a Pt(110)/MgO(110) substrate, and the four peaks at 31.5°, 62.2°, 65.7°, and 67.2° are attributable to $BaTiO_3$(110), MgO(220), $BaTiO_3$(220), and Pt(220) refraction, respectively. This XRD pattern can be indexed to $BaTiO_3$, MgO, and Pt. Strong (*h h 0*) reflections were observed for the $BaTiO_3$ deposited on the Pt(110)/MgO(110) substrate, indicating that the perovskite $BaTiO_3$(110) was heteroepitaxially grown on the Pt(110)/MgO(110). Compared with the 200 peak of the $BaTiO_3$(100) film, the 220 peak of the $BaTiO_3$ (110) film is slightly splitted that the $BaTiO_3$ (110) thin film confirmed to be pseudo-tetragonal perovskite $BaTiO_3$. The lattice constant of the $BaTiO_3$(110) film was calculated to be 0.4170 nm that indicates the lattice of the $BaTiO_3$(110) film is expanded compared with the cubic perovskite $BaTiO_3$. These slight peak split and lattice expansion could be related to the biaxial growth strain.

Figure 1(c) shows the XRD pattern of $BaTiO_3$ deposited on the Pt(111)/MgO(111) substrate, and the three peaks at 36.9°, 38.9°, and 39.6° are attributable to MgO(111), $BaTiO_3$(111), and Pt(111) refraction, respectively. This XRD pattern can be indexed to $BaTiO_3$, MgO, and Pt. Strong (111) reflections were observed for $BaTiO_3$ deposited on the Pt(111)/MgO(111) substrate, indicating that the perovskite $BaTiO_3$(111) was heteroepitaxially grown on the Pt(111)/MgO(111). The lattice constant of the $BaTiO_3$(111) film was calculated to be 0.4249 nm that indicates the lattice of the $BaTiO_3$(111) film is expanded compared with the cubic perovskite $BaTiO_3$.

The tensile stress in the plane of the growth direction in each film is estimated by using lattice expansion from XRD measurement results. The elastic constants (C_{11}, C_{12}, C_{44}) of cubic $BaTiO_3$ single crystal are reported to be 173 GPa, 82 GPa, 108 GPa, respectively.[32] In table S1, the tensile stress in the plane of the growth direction of (100)-, (110)-, and (111)-oriented films are estimated from lattice constant obtained from XRD measurements and elastic constants. From the estimation, the tensile stress of the (110)-oriented film is 5 times and the (111)-oriented film is 8 times higher than that of the (100)-oriented film.

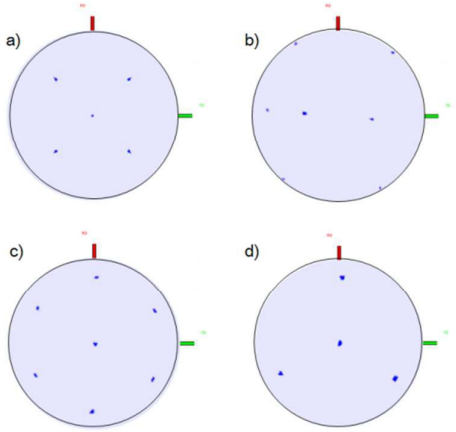

Fig. 2 X-ray pole figures measured with the 111 reflection pattern of (a) $BaTiO_3$(100) film, (b) $BaTiO_3$(110), (c) $BaTiO_3$(111) film, and (d) Pt(111) of the bare Pt(111)/MgO(111) substrate.

Figure 2(a, b, and c) shows an X-ray pole figure measured at a fixed 2θ angle corresponding to the 111 reflection of the $BaTiO_3$(100) film, $BaTiO_3$(110) film, and $BaTiO_3$(111) film, respectively. In figure 2(a), a four-fold symmetry and pole were observed. The pole figure measurement result indicated that a (100) three-axis-oriented $BaTiO_3$ thin film was deposited on the Pt(100)/MgO(100) substrate.

In figure 2(b), the pole figure measurement result indicated that a (110) three-axis-oriented $BaTiO_3$ thin film was deposited on the Pt(110)/MgO(110) substrate. In figure 2(c), six-fold symmetry and a pole were observed. When the $BaTiO_3$ film is (111) three-axis-oriented, three-fold symmetry and a pole must be obtained from the pole figure measurement, so an X-ray pole figure of the bare Pt(111)/MgO(111) substrate was measured to reveal $BaTiO_3$(111) film growth. Figure 2(d) shows an X-ray pole figure measured at a fixed 2θ angle corresponding to the *111* reflection of the Pt(111) of the bare Pt(111)/MgO(111) substrate. Three-fold symmetry and a pole were observed, indicating that the Pt(111) substrate layer is a three-axis-oriented single crystal similar to the film. The pole figure measurement results of the $BaTiO_3$(111) and Pt(111) reveal a 60° rotated twinned $BaTiO_3$(111) film growth on the three-axis-oriented Pt(111) layer.

FE-SEM cross-sectional images were taken to evaluate the morphology of the obtained films. The morphology of the $BaTiO_3$ films changes according to the orientation and crystallinity of the $BaTiO_3$ films. Common grain-structured $BaTiO_3$ film layers are randomly oriented, columnar-structured $BaTiO_3$ film layers are one-axis oriented and densified $BaTiO_3$ film layers without visible grain boundaries are three axis oriented. [28-30,33] Figure S1(a, b, and c) shows the cross-sectional FE-SEM image of a $BaTiO_3$(100) film on a Pt(100)/MgO(100) substrate, $BaTiO_3$(110) film on a Pt(110)/MgO(110) substrate, and $BaTiO_3$(111) on a Pt(111)/MgO(111) substrate, respectively, and the thicknesses of the $BaTiO_3$ thin films were confirmed at 165 nm, 160 nm, and 165 nm, respectively. These $BaTiO_3$ thin films did not show the presence of grain boundaries, which are the typical morphology for three-axis oriented films.[31] The FE-SEM cross-sectional images indicate that highly densified and orientation-controlled films were obtained by our method.

Figure S2(a) shows cross-sectional TEM images of the $BaTiO_3$ thin film deposited on a Pt(100)/MgO(100) substrate. The $BaTiO_3$ layer is effectively single-crystal-like with no visible grain boundary. Figure S2(b) shows the cross-sectional bright-field TEM image of the boundary of the Pt sputtered film and $BaTiO_3$ thin film. The $BaTiO_3$ layer is highly epitaxial and effectively single-crystal-like with no visible grain boundary. The SAED patterns from the boundary of the Pt sputtered film and $BaTiO_3$ thin film are shown in figure S2(c). The SAED patterns were observed when the electron beam was parallel to the [010] axis of the Pt sputtered film. Figure S2(c) indicates that the spots of Pt and $BaTiO_3$ overlap and have the same preferred orientation of (100). The TEM observations indicate that a (100) three-axis-oriented $BaTiO_3$ thin film was deposited on the Pt(100)/MgO(100) substrate. These results are consistent with the results of the XRD pattern and X-ray pole figure measurement.

Figure S3(a) shows cross-sectional TEM images of the $BaTiO_3$ thin film deposited on the Pt(110)/MgO(110) substrate. The morphology of the $BaTiO_3$ thin film deposited on the Pt(110)/MgO(110) substrate is similar to that of the $BaTiO_3$ thin film deposited on the Pt(100)/MgO(100) substrate. Figure S3(b) shows the cross-sectional bright-field TEM image of the boundary of the Pt sputtered film and the $BaTiO_3$ thin film. The $BaTiO_3$ layer is highly epitaxial and effectively single-crystal-like with no visible grain boundary. The SAED patterns from the boundary of the Pt sputtered film and $BaTiO_3$ thin film are shown in figure S3(c). The SAED patterns were observed when the electron beam was parallel to the [010] axis of the Pt sputtered film. Figure S3(c) indicates that spots of Pt and $BaTiO_3$ overlap and have a same preferred orientation of (110). These results indicates that a (110) three-axis-oriented $BaTiO_3$ thin film was deposited on the Pt(110)/MgO(110) substrate. These results are consistent with the results of the XRD pattern and X-ray pole figure measurement.

Figure S4(a) shows cross-sectional TEM images of the $BaTiO_3$ thin film deposited on the Pt(111)/MgO(111) substrate. The $BaTiO_3$ layer is effectively single-crystal-like with no visible grain boundary. Figure S4(b) shows the cross-sectional bright-field TEM image of the boundary of the Pt sputtered film and $BaTiO_3$ thin film. The $BaTiO_3$ layer is highly epitaxial and effectively single-crystal-like with no visible grain boundary. The SAED patterns from the boundary of the Pt sputtered film and $BaTiO_3$ thin film are shown in figure S4(c). SAED patterns were taken when the electron beam was in parallel to the [112] axis of the Pt sputtered film. Figure S4(c) indicates that the spots of Pt and $BaTiO_3$ overlap and have the same preferred orientation of (111).

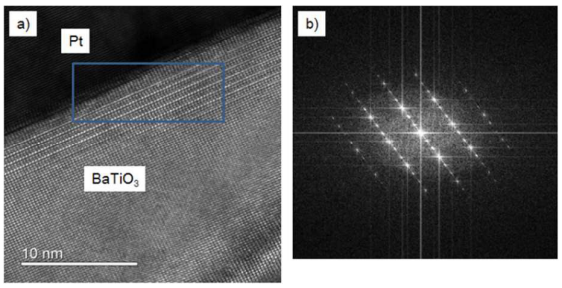

Fig. 3(a) Bright-field Cs-STEM image of the boundary of the $BaTiO_3$(111) film and Pt(111) film and (b) FFT pattern of the Cs-STEM image surrounded by a rectangle part in figure 3(a).

The Cs-STEM observations were carried out to reveal the twin growth indicated by X-ray pole figure measurement.

Figure 3(a) shows the cross-sectional bright-field Cs-STEM image of the boundary of the $BaTiO_3$(111) film and Pt(111) film. The Cs-STEM image shows multiple periods of contrast change in the $BaTiO_3$ layer. Figure 3(b) is the fast Fourier transform (FFT) pattern of the Cs-STEM image and shows multiple periods of contrast change. The weak spikes in the FFT pattern show a three-fold cycle and 3/2-fold cycle. These weak spikes indicate the appearance of a forbidden reflection caused by multiple diffraction, which indicates twin growth of the $BaTiO_3$.[34] These results are consistent with the results of the X-ray pole figure measurement that twined $BaTiO_3$(111) growth on the Pt(111) layer.

The capacitance of the obtained $BaTiO_3$ films was measured at 1 kHz and 0.1 V. The dielectric constants were calculated from the average of measured capacitance and thickness as shown in Table S2. The (110)-oriented and (111)-oriented $BaTiO_3$ films have dielectric constants that are approximately twice that of the (100)-oriented $BaTiO_3$ film. The morphology and density of the films observed from the FE-SEM images and TEM images are similar; therefore the differences in the dielectric constants were assumed to be enhanced by differences in the orientation of the $BaTiO_3$.

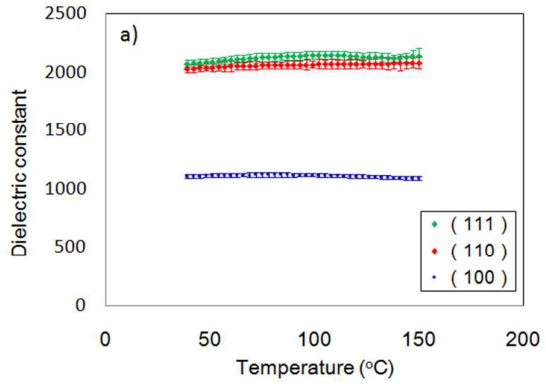

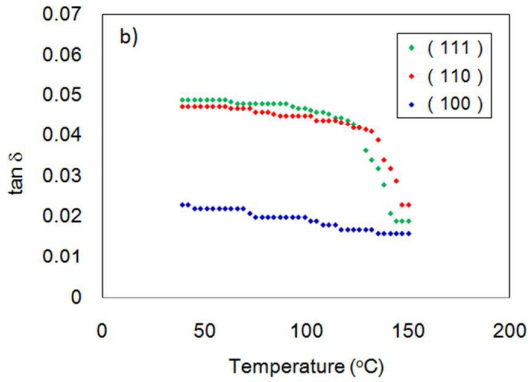

Fig. 4 Temperature dependence of (a) the dielectric constant, (b) tangent delta in the $BaTiO_3$ films.

The temperature dependence of the dielectric constant and tangent delta in the $BaTiO_3$ films is shown in figure 4. The dielectric constant was measured at 1 kHz and 0.1 V and zero biased from 20 °C to 150 °C. Temperature dependencies of the dielectric constant of the $BaTiO_3$ films were stable at all measured temperatures, which indicates that a phase transition does not occur in the measured temperature range. The Curie temperature is the transition temperature between the ferroelectric and non-ferroelectric structures of $BaTiO_3$, and it is known to be at approximately 120 °C for $BaTiO_3$. This phase transition of $BaTiO_3$ is well known, and tetragonal perovskite transitions to pseudocubic perovskite with increases of temperature.[35] This result is consistent with the XRD result in which $BaTiO_3$ films were not tetragonal perovskite but pseudocubic perovskite at room temperature because pseudocubic perovskite $BaTiO_3$ does not exhibit a phase transition with increases from Curie temperature. The temperature dependence of the dielectric constant indicates that the obtained $BaTiO_3$ films were pseudocubic perovskite at all measured temperature ranges; therefore, the temperature dependencies of the dielectric constant of the $BaTiO_3$ films were stable at all measured temperatures.

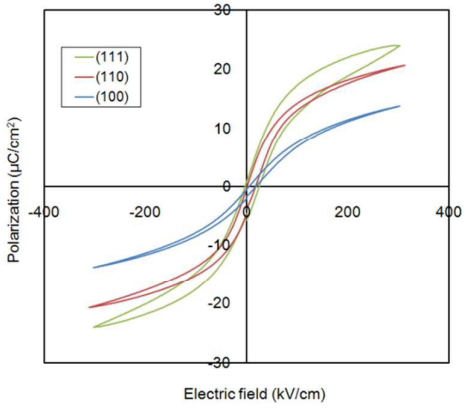

Fig. 5 P-E hysteresis loops of the $BaTiO_3$ films in the MDM capacitors.

Figure 5 shows the P-E hysteresis loop of the $BaTiO_3$(100) film, $BaTiO_3$(110) film, and $BaTiO_3$(111) film in the MDM capacitor after the P-E loops were run for several times. The $BaTiO_3$(100) film, $BaTiO_3$(110) film, and $BaTiO_3$(111) film had remnant and corresponding coercive fields of 0.9 $\mu C/cm^2$ and 6.6 kV/cm, 1.9 $\mu C/cm^2$ and 8.2 kV/cm, 3.0$\mu C/cm^2$ and 13.7 kV/cm, respectively. The hysteresis loops indicated that the ferroelectric properties of the $BaTiO_3$(110) film and $BaTiO_3$(111) film were enhanced compared with the ferroelectric properties of the $BaTiO_3$(100) film. This result is consistent with the first principle calculation by Gui et al.,[24] in which the dielectric constant of the (110)-oriented of $BaTiO_3$ film exhibited a significant enhancement compared with the dielectric constant of the (100)-oriented of $BaTiO_3$ because of the induced compressive biaxial strain perpendicular to the growth direction.

The DC resistivity of thin films prepared from a variety of film orientations measured at 300 kV/cm is shown in Table S3. The resistivity of $BaTiO_3$(100) film, $BaTiO_3$(110) film, and $BaTiO_3$(111) film were 5.91 x 10^8 Ω·cm, 4.48 x 10^8 Ω·cm, 8.70 x 10^7 Ω·cm, respectively. The $BaTiO_3$(111) film possesses lower resistivity compared with the resistivity of the $BaTiO_3$(100) film. This decreased resistivity has caused the P-E loop to look inflated and not have nicely pinched ends, increasing the values for coercive field and remnant polarization.

We assume that tensile stress in the plane of the growth direction that was induced during the twinned growth of $BaTiO_3$(111) enhanced the ferroelectric properties of the and lowered resistivity compared with the ferroelectric properties of the (100)-oriented $BaTiO_3$ film.

Conclusions

The (100)-, (110)-, and (111)-oriented $BaTiO_3$ films were successfully synthesized on a Pt-coated MgO substrate by CSD processing. The electric properties of the fabricated $BaTiO_3$ thin films were evaluated and revealed that the ferroelectric properties of the $BaTiO_3$(110) film and $BaTiO_3$(111) film are enhanced compared with the $BaTiO_3$(100) film. The enhancement of the ferroelectric properties is assumed to be induced by tensile stress in the same plane as the growth direction. Furthermore, dielectric constants as high as 2000 with stable temperature-dependent $BaTiO_3$ films were produced by a mass production procedure that will benefit thin-film capacitors in the near future.

Acknowledgements

The authors thank Masato Adachi for the X-ray pole figure measurements and Tomonori Muraki for the TEM measurement.

Notes and references

[a] Murata Manufacturing Co., Ltd.
10-1, Higashikotari, 1-chome, Nagaokakyo-shi, Kyoto 617-8555 Japan
E-mail:hosokura@murata.com

†Electronic Supplementary Information (ESI) available: [Figure S1 cross-sectional FE-SEM image of the $BaTiO_3$ films; Figure S2-S4 cross-sectional TEM images of the $BaTiO_3$ films; Table S1 Elastic constants and tensile stress in the plane of the growth direction of (100)-, (110)-, and (111)-oriented film. ; Table S2 the capacitance of the obtained $BaTiO_3$ films measured at 1 kHz and 0.1 V. ; Table S3 DC resistivity of thin films prepared from a variety of film orientations measured at 300 kV/cm.] See DOI: 10.1039/x0xx00000x

1 J. F. Scott, *Science,* 2007, **315**, 954-959.
2 K.-H. Chen, Y.-C. Chen, Z.-S. Chen, C.-F. Yang and T.-C. Chang, *Appl. Phys. A*, 2007, **89**, 533-536.
3 Y. Takeshima, K. Shiratsuyu, H. Takagi and Y. Sakabe, *Jpn. J. Appl. Phys*., 1997, **36**, 5870-5873.
4 Z. Liu, P.-T. Lin, W. B. Wessels, F. Yi and S.-T. Ho, *Appl. Phys*. Lett., 2007, **90**, 201104.
5 V. S. Dharmadhikari and W. W. Grannemann, *J. Appl. Phys*., 1982, **53**, 8988-8992.
6 J. H. Kim and S. Hishita, *J. Mater. Sci*., 1995, **30**, 4645-4650.
7 S. Canulescu, G. Dinescu, G. Epurescu, D. G. Mateia, C. Grigoriua, F. Craciunb, P. Verardib and M. Dinescu, *Mater Sci. Eng. B,* 2004, **109,** 1, 160-166.
8 G. M. Norton, K. P. B. Cracknell and B. C. Carter, *J. Am. Ceram Soc*., 1992, **75**, 1999-2002.
9 G. M. Norton, C. Scarfone, J. Li, B. C. Carter and W. J. Mayer, *J. Mater. Res*., 1991, **6**, 2022-2025.
10 T. Chiba, K. Itoh and O. Matsumoto, *Thin Solid Films,* 1997, **300**, 1, 6-10.
11 G. M. Norton and B. C. Carter, *J. Mater. Res.,* 1990, **5**, 2762-2765.
12 C. S. Chern, J. Zhao, L. Luo, P. Lu, Y. Q. Li, P. Norris, B. Kear, F. Cosandey, C. J. Maggiore, B. Gallois and B. J.Wilkens, *Appl. Phys. Lett*., 1992, **60**, 1144.
13 D. L. Kaiser, M. D. Vaudin, L. D. Rotter Z. L., Wang, J. P. Cline, C. S. Hwang, P. B. Marinenko and J. G. Gillen, *Appl. Phys. Lett.,* 1995, **66**, 2801-2803.
14 Y. S. Yoon, M. N. Kang, H. S. Shin, S. S. Yom, T. W. Kim, J. Y. Lee, D. J. Choi and S.-S. Baek, *J. Appl. Phys*., 1993, **73**, 1547.
15 U. Hasenkox, S. Hoffmann and R. Waser, *J. Sol-Gel Sci. Technol*., 1998, **12**, 67-79.
16 R. Roy, *Science*, 1987, **238**, 1664-1669.
17 H. Liu, P. Yang, Z. Fan, A. Kumar, K. Yao, K. P. Ong, K. Zeng and J. Wang, *Phys. Rev. B*, 2013, **87**, 220101.
18 K. Iijima, T. Terashima, Y. Bando, K. Kamigai and H. Terauchi, *J. Appl. Phys*., 1992, **72**, 2840-2845.
19 H. Tabata, H. Tanaka and T. Kawai, *Appl. Phys. Lett*., 1994, **65**, 1970-1972.
20 T. Tsurumi, T. Suzuki, M. Yamane and M. Daimon, *Jpn. J. Appl. Phys. Part 1*, 1994, **33**, 5192-5195.
21 T. Shimizu, D. Suwama, H. Taniguchi, T. Taniyama and M. Itoh, *Appl. Phys. Express*, 2013, **6**, 015803.
22 K. J. Choi, M. Biegalski, Y. L. Li, A. Sharan, J. Schubert, R. Uecker, P. Reiche, Y. B. Chen, X. Q. Pan, V. Gopalan, L.-Q. Chen, D. G. Schlom and C. B. Eom, *Science*, 2004, **306**, 1005-1009.
23 T. Hosokura, N. Iwaji, T. Nakagawa, A. Ando, H. Takagi, Y Sakabe, and K. Hirao, *Cryst. Growth Des*., 2011, **11**, 10, 4253-4256.
24 Z. Gui, S. Prosandeev and L. Bellaich, *Phys. Rev. B*, 2011, **84**, 214112.
25 T. Schneller and R. Waser, *Ferroelectrics*, 2002, **267**, 293-301.
26 F. F. Lange, *Science*, 1996, **273**, 903-909.
27 T. Hosokura, A. Ando and Y. Sakabe, *Key Eng. Mater*., 2006, **320**, 81-84.

28 C. L. Jia, K.Urban, S. Hoffmann and R. Waser, *J. Mater. Res*., 1998, **13**, 2206-2217.
29 W. R. Schwartz, *Chem. Mater.*, 1997, **9**, 2325-2340.
30 W. R. Schwartz, P. G. Clem, A. J. Voigt, R. E. Byhoff, V. M. Stry, J. T. Headley and A. N. Missert, *J. Am Ceram Soc*., 1999, **82**, 9, 2359-2367.
31 J. J. Wang, F. Y. Meng, X. Q. Ma, M. X. Xu, and L. Q. Chen, *J. Appl. Phys*., 2010, **108**, 034107.
32 D. Berlincort, and H. Japeze, *Phys. Rev.*, 1985, **111**, 143-148.
33 T. Hosokura, K. Kageyama, H. Takagi and Y. Sakabe, *J. Am. Ceram. Soc*., 2009, **92**, 1, 253-255.
34 H. Oppolzer and H. Schmelz, *J. Am. Ceram. Soc*., 1983, **66**, 6, 444-446.
35 M. G. Harwood, P. Popper and D. F. Rushman, *Nature*, 1947, **160**, 58-59.

A table of contents

We synthesized orientation-controlled (100), (110), and (111) $BaTiO_3$ films by the CSD method and revealed the dielectric properties the films.